Surface-Confined Nanoclays in Ethylene Butyl Acrylate Copolymer: Toward Smarter Flame Retardancy

Macromolecular Materials and Engineering

Macromolecular Materials and Engineering Open Access

www.mame-journal.de

RESEARCH ARTICLE OPEN ACCESS

Surface-Confined Nanoclays in Ethylene Butyl Acrylate Copolymer: Toward Smarter Flame Retardancy

Alberto Frache | Eleonora Lorenzi | Fulvia Cravero | Rossella Arrigo

Department of Applied Science and Technology, Politecnico di Torino, Alessandria, Italy

Correspondence: Alberto Frache (alberto.frache@polito.it)

Received: 21 October 2025 | **Revised:** 9 January 2026 | **Accepted:** 19 January 2026

Keywords: cast extrusion | coatings | combustion behavior | cone calorimeter | nanocomposites

ABSTRACT

This study explores the development of nanostructured flame-retardant systems using ethylene-butyl acrylate (EBA) copolymer and nanoclays. This was achieved following two strategies: namely, the incorporation of the nanofiller into the bulk material or its confinement to the surface through the utilization of coatings. First, the effectiveness of the bulk approach was evaluated. To this aim, 4 wt.% nanoclays were embedded within EBA, resulting in a 50% reduction in peak heat release rate and a significant delay in flame-out time when compared to the unfilled copolymer. Then, films containing 4 wt.% nanoclay with a thickness of 300 μm produced via compression molding or cast extrusion, were applied as surface coatings to unfilled EBA substrates, yielding an overall clay content of 0.36 wt.% of the total sample. Despite the reduced nanoclay content, the surface confinement proved to be more effective than the bulk incorporation in delaying ignition time (an increase of 20% and 50% compared to the bulk nanocomposite and neat copolymer, respectively), suggesting more efficient initial protective action. Overall, the obtained results indicate that the nanoclay surface localization leads to slower fire propagation and improved fire safety while preserving polymer bulk properties.

1 | Introduction

In many application fields, such as construction, transportation, and electrical/electronics, the use of flame-retardant materials is essential to meet safety standards and reduce risks associated with highly combustible materials. Polymer materials are among the most widely used in these sectors, but also highly flammable. For this reason, significant efforts have been devoted to improving their flame resistance. The most common approach involves the incorporation of flame-retardant additives into the polymeric matrix. Halogenated compounds (e.g., bromine and chlorine-based) have long been the most commonly exploited due to their effectiveness and low cost. However, environmental and toxicity concerns have driven research toward non-halogenated alternatives, such as phosphorus compounds, inorganic hydroxides, and intumescent systems [1]. While these are effective, they often require high loadings (20–60 wt.%), which can negatively affect the mechanical properties and processability of the material. On the other hand, the use of nanofillers is more advantageous from this perspective, as amounts ranging from 0.5 to 5 wt.% are already sufficient to provide good fire performances. In fact, the flame-retardant action provided by organo-modified nanoclays is a well-established phenomenon, extensively documented in the literature [2–4]. This effect can be attributed to both physical and chemical mechanisms. The physical mechanism involves the formation of a protective layer through the migration of the clay lamellae to the surface and the ablation of the polymer. The chemical mechanism, on the other hand, consists of a catalytic effect, which promotes charring and the formation of a protective, coat-like char. This char acts as both a thermal shield and a barrier to the mass transport of degradation products, thereby reducing the polymer's further exposure to heat and oxygen.

Since polymer flammability is primarily a surface-related property, and the surface of the substrate plays a central role in both degradation and ignition, the surface-confinement of the flame-retardant action through the use of coatings can be an interesting and effective strategy [5–9]. In fact, this approach allows reducing even more the filler loadings, while maintaining unchanged the bulk properties of the substrate. Particularly, this last is especially helpful in applications where it is crucial to preserve the properties of the polymer matrix, such as in the textile industry (e.g., safety garments or furniture) or the electrical field (e.g., cables and wires). In this context, Gallo et al. [10] prepared a double-component laminate structure by coupling a superficial flame retardant layer (containing a combination of a phosphorus-based flame retardant and nanometric metal oxide) with a fiber-reinforced core. The results of cone calorimeter tests showed that, compared to the bulk formulation, the laminate structures exhibited similar or better resistance to fire, with a drastic reduction in the peak heat release rate and in the fire spread indices. Recently, Tabaka et al. [11] formulated a laminate structure in which different types of flame retardants were concentrated in the surface layer of a two-layer glass fibre-reinforced polybutylene terephthalate. It was demonstrated that increasing the flame retardant concentration in the top layer significantly reduced both the peak heat release rate and the maximum average rate of heat emission, thus confirming the effectiveness of the proposed approach. Furthermore, from a general point of view, various strategies for applying flame retardant coatings have been explored in the literature, including the deposition of silica-based thin films via layer-by-layer assembly onto synthetic or natural textile fabrics [12], and the use of intumescent coatings [13].

As previously mentioned, one of the fields where it is crucial to ensure good flame-retardant properties, specifically by delaying the ignition of the material while simultaneously maintaining the properties of the initial polymer matrix, is the electrical sector, particularly for the production of wire and cable jackets. In this field, the use of ethylene copolymers, such as polyethylene-vinyl acetate (EVA) and ethylene-butyl acrylate (EBA), is very common due to their great flexibility and rubber-like behavior. While the combustion behavior of EVA and the improvement of its flame-retardant properties through various additive systems have been extensively studied [14–19], EBA remains much less well-known, and the literature on this polymer is very limited. EBA differs from EVA due to the presence of butyl acrylate instead of vinyl acetate, resulting in a longer side chain. The butyl group makes EBA less polar and, consequently, less hygroscopic than EVA, which could actually offer a significant advantage in applications such as electrical wire and cable coatings. Existing literature on EBA primarily focuses on its thermal degradation [20, 21], while studies on its combustion behavior are almost absent. Karlsson et al. [22] studied halogen-free flame-retardant materials consisting of ethylene copolymers, calcium carbonate, and silicone elastomer. Besides, the synergistic effect of an intumescent formulation with organophilic clays or a silicone-containing macromolecular charring agent were studied by Ribeiro et al. [23] and Huo et al. [24], respectively. However, no studies have been conducted on the combustion behavior of EBA-based systems containing only nanoclay.

Considering this aspect, along with the advantages of using flame-retardant coatings, this study evaluated the effectiveness of nanostructured films for developing EBA-based flame-retardant systems. First, the influence of nanoclay on the fire-retardant properties of the polymer matrix was assessed by producing an EBA-based nanocomposite containing 4 wt.% nanofillers. Then, a surface approach was explored, by applying EBA/nanoclay films (produced through either compression molding (CM) and cast extrusion (CE)) onto unfilled EBA specimens.

Pristine EBA and EBA-based nanocomposites (both bulk and films) were preliminary characterized through thermal, rheological and morphological analyses. Additionally, the flame-retardant properties of all the formulated systems were evaluated using cone calorimeter tests. The results showed that the application of the nanoclay-rich surface layer was effective in enhancing the fire performance of the material, leading to an increase of the time to ignition and a reduction of the peak of heat release rate, as compared to uncoated EBA. Overall, the obtained results allowed highlighting the potential of the coating approach to improve fire safety, while minimizing the required amount of nanoclays, thereby preserving the bulk properties of the polymer matrix.

2 | Materials and Methods

2.1 | Materials

The polymer used as a matrix is Ethylene Butyl Acrylate (EBA) Lucofin 1400MN (supplied by Lucobit, Wesseling, Germany). It is a polyethylene (PE)—butyl acrylate (BA) copolymer characterized by a BA content of 17% and having a melt flow index of 7.0 g/10 min (190°C, 2.16 kg). In addition, the commercially available masterbatch Lucofin 7500 (supplied by Lucobit, Wesseling, Germany) was used to produce the nanocomposites.

2.2 | Processing and Preparation of Specimens

The EBA/nanoclay nanocomposite containing 4 wt.% of nanoclay was prepared using a Leistritz (Nürnberg, Germany) ZSE18/40D twin-screw extruder. The screw speed was maintained at 150 rpm, while the feed rate was 1 kg/h. The temperature profile (from the hopper to the die) was 160°C/165°C/170°C/175°C/180°C/180°C/180°C/, and 180°C. At the die exit, the extrudate was cooled to room temperature in a water bath and pelletized.

A Wittmann-Battenfeld (Kottingbrunn, Austria) Smart Power 50 injection molding machine was used to produce the 100 × 100 × 3 mm ISO5660 cone calorimeter specimens. The same processing conditions (namely, barrel temperature profile: 200–190–180°C from hopper to die and mold temperature: 30°C) were used to produce both pristine EBA and EBA/nanoclay specimens.

In addition, the EBA/nanoclay nanocomposite was used to produce films through two approaches. First, 100 × 100 mm films were prepared by compression molding (CM) using a Collins (Maitenbeth, Germany) P200T hot plate press. The process was performed at 130°C and 50 bar with a 2 min maintenance time. Furthermore, the EBA/nanoclay material was also processed by cast extrusion (CE) in an EUR.EX.MA Srl (Varese, Italy) single-screw extruder (D = 25 mm, L/D = 32) equipped with

TABLE 1 | Nomenclature of the produced specimens.

Code	Description	Schematic representation
EBA	Pristine EBA specimens processed by injection molding	
EBA/nanoclay_bulk	EBA + 4 wt.% nanoclay nanocomposite processed by injection molding	
EBA/nanoclay_coating_CM	Pristine EBA specimen coated with the compression molded film of EBA + 4 wt.% nanoclay nanocomposite	
EBA/nanoclay_coating_CE	Pristine EBA specimen coated with cast extruded film of EBA + 4 wt.% nanoclay nanocomposite	

a conventional three-compression zones screw with a general-purpose design and a flat die. The screw speed was maintained at 60 rpm and the temperature at 185°C along the barrel. The film was obtained using to an EUR.EX.MA Srl (Varese, Italy) calender with a three-roll sheet stack arrangement (roll temperature = 30°C).

Both CM and CE films are characterized by a thickness of 300 μm.

Finally, the films obtained with CM or CE were applied to the injection molded specimens of pristine EBA through a compression molding process, using a Collins (Maitenbeth, Germany) P200T hot plate press performed at 90°C and 20 bar for 30 s.

The codes hereinafter used to name the different produced samples are summarized in Table 1.

2.3 | Characterization Techniques

Thermal analyses were performed using a DSC TA Q20 (TA Instruments, New Castle, DE, USA) having the chamber purged by nitrogen. Samples of 8 ± 1 mg were used. The materials were subjected to the following thermal cycle: a first heating ramp from −30°C to 220°C, a cooling ramp from 220°C to −30°C and a second heating ramp from −30°C to 220°C. During all the steps, the heating/cooling rate was maintained at 10°C/min.

The crystallization temperature (Tc) was evaluated as the maximum of the exothermic peak recorded during the cooling ramp, while the melting temperature (Tm) was obtained from the maximum of the endothermic peak in the second heating ramp. Furthermore, the integral of the area under this endothermic peak corresponded to the melting enthalpy (ΔHm). In order to evaluate the crystallinity content, it has to be taken into account that EBA is a polyethylene-butyl acrylate copolymer and only polyethylene is semi-crystalline while butyl acrylate is amorphous. Therefore, the ΔHm refers to the PE content [25]. The crystallinity content was calculated according to Equation (1):

$$\chi_c = \frac{\Delta H_m}{0.83 \cdot \Delta H_m^0 \cdot (1-x)} \cdot 100 \quad (1)$$

where: χ_c is the crystallinity content, ΔH_m is the melting enthalpy, 0.83 is the coefficient related to the PE content over EBA, ΔH_m^0 is the melting enthalpy of the 100% crystalline polyethylene (277 J/g [26]), x represents the nanoclay content.

Thermogravimetric analyses were performed on samples of 10 ± 1 mg using a Perkin Elmer (Shelton, CT, USA) TGA 4000 coupled with a Perkin Elmer (Shelton, CT, USA) Fourier Transform Infrared (FTIR) Spectrometer Spectrum Two. The tests were performed in either inert (nitrogen flow of 35 mL/min) or oxidative (air flow of 30 mL/min) atmospheres. A heating rate of 10°C/min was used for the heating ramp between 50°C and 700°C. Besides, the evolved gases were transferred to the gas cell, maintained at a temperature of 280°C, and the FTIR spectra were collected in continuous time-resolved scans at a resolution of 4 cm^{-1}.

The rheological behavior of EBA and EBA/nanoclay nanocomposite was evaluated using an ARES (TA Instruments, New Castle, DE, USA) strain-controlled rheometer in a parallel plate geometry (plate diameter = 25 mm, gap = 1 mm). Frequency sweep tests were performed in nitrogen at 180°C with a frequency ranging from 100 to 0.1 rad/s. For both materials, the strain amplitude was selected to be within the linear viscoelastic region (preliminary assessed through strain sweep measurements carried out at 180°C and a frequency of 10 rad/s).

Combustion behavior was evaluated with a Noselab Ats (Monza, Italy) cone calorimeter, according to the ISO5660 standard. Samples of 100 × 100 × 3 mm were tested under a radiant heat flux of 35 kW/m^2 at a distance of 25 mm. To ensure reliability, three replicates were performed for each system, allowing to estimate the time to ignition (TTI), the heat release rate (HRR), the peak of the heat release rate (pkHRR), the time of the pkHRR (tpeak), the total heat release (THR), the total smoke release (TSR) and the time to flame out (TTFO). Besides, to evaluate the fire hazard, the fire growth rate index (FIGRA) was calculated according to Equation (2), while for the fire protection index (FPI) Equation (3) was used [27]:

$$FIGRA = \frac{pkHRR}{t_{peak}} \quad (2)$$

$$FPI = \frac{pkHRR}{TTI} \quad (3)$$

A Zeiss (Oberkochen Germany) EVO 15 Scanning Electron Microscope (SEM) (20 kV beam voltage and 8.5 mm working

TABLE 2 | Main thermal properties of EBA and EBA/nanoclay nanocomposite.

Material	Tc (°C)	Tm (°C)	ΔHm (J/g)	χ_c (%)
EBA	74	94	57	25
EBA/nanoclay	76	95	49	22

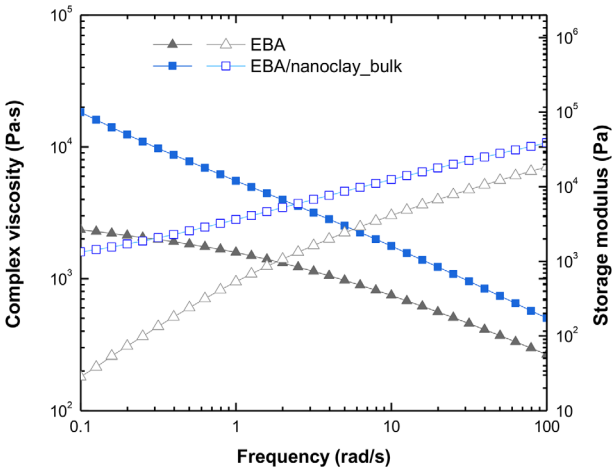

FIGURE 1 | Complex viscosity (full symbols) and storage modulus (empty symbols) as a function of frequency for unfilled EBA and EBA/nanoclay nanocomposite.

distance) was used for morphological analysis. The sections to be observed were obtained by fracturing the specimens in liquid nitrogen. It is important to note that the CE film was fractured parallel to the machine direction. In addition, the residues of the cone calorimeter test were collected, and the surface was examined. In all cases, the samples were gold sputtered prior to morphological analysis.

3 | Results and Discussion

3.1 | Preliminary Characterization of EBA/Nanoclay Nanocomposite

The thermal behavior of both EBA and EBA/nanoclay nanocomposite was characterized by DSC analysis and the main thermal properties are reported in Table 2. The comparison between the two materials clearly demonstrates that the presence of 4 wt.% nanofiller does not significantly affect the crystallization behavior of the polymeric matrix, in agreement with the literature on similar systems [28–31].

The complex viscosity curve of EBA, obtained through dynamic frequency sweep tests and reported in Figure 1, testifies for the pristine polymer a slight non-Newtonian behavior. In fact, in the low frequency region, a not fully developed Newtonian plateau can be observed, followed by a mild shear thinning behavior at higher frequencies. On the other hand, the introduction of the nanoclays induces an increase of the complex viscosity in the whole investigated frequency interval. In particular, this phenomenon is more pronounced in the low frequency range, leading to an amplification of the non-Newtonian features as compared to the unfilled matrix. Furthermore, the embedded nanofillers also affect the storage modulus trend as a function of the frequency. Once again, the differences between the nanocomposite and the pristine EBA are more remarkable in the terminal region (i.e., at low frequencies), where a significant modification of the frequency dependence of the modulus curve can be observed. The rheological response of EBA/nanoclay nanocomposite suggests that the nanofillers are able to interfere with the dynamics of the matrix macromolecules, hampering their complete re-laxation. Usually, the noticed behavior is attributed to the occurrence of strong interactions at the interface, leading to the formation of interconnected polymer/nanofiller and nanofiller/nanofiller networks, strongly affecting the macromolecules dynamics [32]. Additionally, in the case of nanocomposites containing layered nanofillers, the incomplete relaxation of the polymer chains can be associated with the formation of intercalated structures and/or intercalated/exfoliate hybrids, causing a restriction of the dynamic response of the matrix macromolecules [33].

The thermal and thermo-oxidative degradation of both EBA and EBA/nanoclay was evaluated through TGA-FTIR analyses, and the obtained results are depicted in Figure 2. As can be appreciated in Figure 2A, when the analysis is performed on the pristine matrix in nitrogen, a single degradation step is present. The T_{ONSET} (i.e., the onset of degradation evaluated as the temperature at which a loss of 2 wt.% occurs) is 385°C, while the temperature corresponding to the maximum rate of weight loss (T_{MAX}) is 451°C; besides, in accordance with the literature [21], no residue is observed after 500°C.

The evolution of volatile degradation products was also monitored by infrared analysis and the spectra collected at three different, significant temperatures are reported in Figure 2B. Sampling temperatures are highlighted with dots on the corresponding TGA curve (Figure 2A). As known from the literature, the thermal degradation of EBA occurs with the mechanism of ester pyrolysis, resulting in the formation of butene and volatile hydrocarbon species containing carboxyl groups [20, 21, 34, 35].

The formation of butene after the onset of the thermal degradation is mainly confirmed by the presence, in the spectrum collected at 431°C, of the peaks in the range 3000–2750 cm^{-1}, attributed to the CH_2 symmetric and asymmetric stretching [21]. Furthermore, the peaks at 3081 cm^{-1} (= C—H stretching), 1639 cm^{-1} (C = C stretching) and 910 cm^{-1} (C = CH_2 bending), typical of alkenes [21] are also detected. On the other hand, focusing on the wavelength range around 1700 cm^{-1}, the peaks associated with methylene and methyl species have also been attributed to low molecular weight alkanes containing carbonyl groups [36]. In fact, as can be seen from Figure 2B, the peak centered at 1739 cm^{-1}can indicate the presence of ester or aldehyde groups on the volatile products [35, 37].

When the temperature is increased to 451°C (corresponding to T_{MAX}) a substantial growth of the intensity of the peaks related to the CH_2 symmetric and asymmetric stretching is observed. Furthermore, it can be noticed a shift of the peaks attributed to carbonyl-containing species. In particular, two peaks at 1756 and 1714 $cm^{-1}$are recognized. The former denotes the presence of ketones or lactones, whereas the latter a distinctive feature

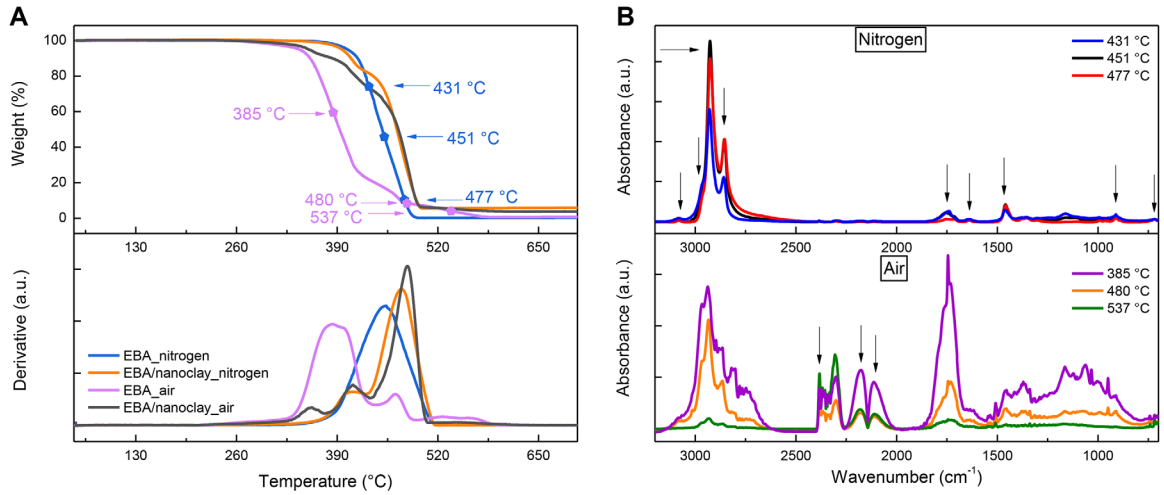

FIGURE 2 | (A) TGA curves and corresponding derivatives for EBA and EBA/nanoclay in inert and oxidative atmospheres. (B) FTIR spectra recorded at different temperatures during TGA measurements.

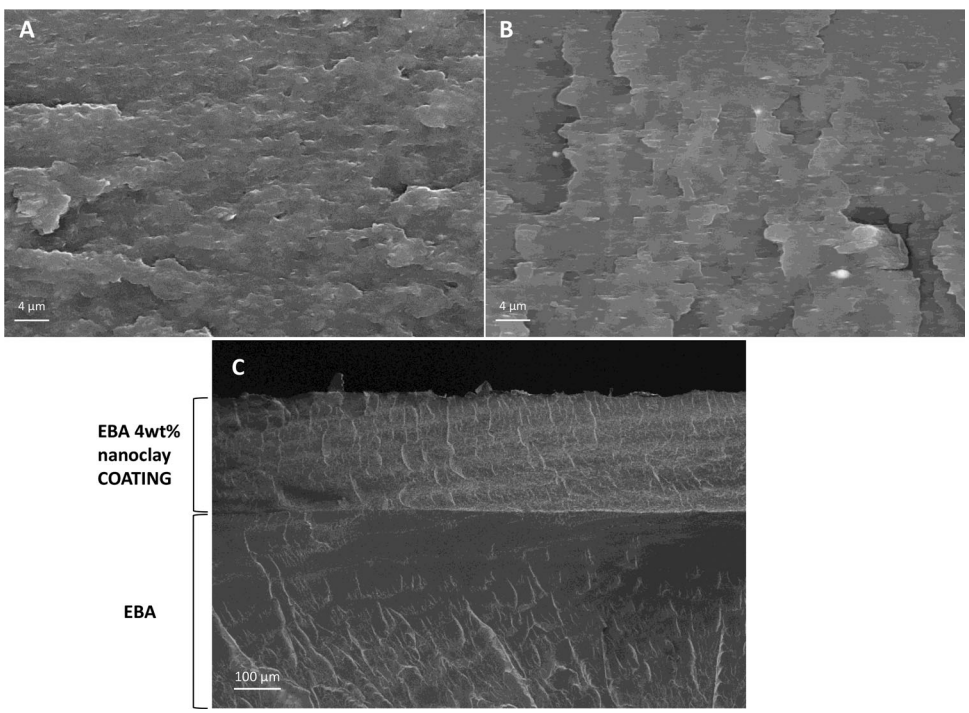

FIGURE 3 | SEM micrographs of (A) compression-molded film, (B) cast-extruded film, (C) EBA/nanoclay_coating CE sample.

of carboxylic acids, which is characteristic of the pyrolysis mechanism occurring on EBA [20, 21, 34, 36]. Finally, at 477°C, the signals associated with carbonyl groups are almost negligible, so the volatile products are mostly alkane/alkene species [21].

A different degradation behavior is observed for EBA in oxidative atmosphere (Figure 2A). First, the T_{ONSET} decreases to 305°C. Besides, three degradation steps can be distinguished, with the main weight loss of about 71% occurring in the first one. Finally, the temperature at which no residue is detected increased to 585°C when compared to the inert atmosphere analysis. In addition, the thermal oxidation of EBA also leads to the formation of volatile products that further oxidize in the gas phase. This is confirmed by the presence in the infrared spectra (Figure 3B) of signals related to the carboxylic group at 1714 $cm^{-1}$and to esters or aldehydes at 1744 cm^{-1} [20, 21, 34, 36, 37]. Furthermore, peaks associated with carbon dioxide (CO_2) and carbon monoxide (CO) are clearly observed between 2400 and 2000 cm^{-1} (Figure 3B). In particular, the signal at 2382 $cm^{-1}$is related to the antisymmetric stretching in CO_2, while those at 2177 and 2114 $cm^{-1}$are due to CO [21, 38–40]. Therefore, according to the infrared spectra of the volatiles formed at 385°C (Figure 3B) and considering the variation of the intensity of the peaks relative to the different species with temperature, it can be concluded that in the first phase of thermal degradation in oxidative atmosphere butene, oxidized low molecular weight chains of hydrocarbons, CO

and CO_2 are released. Subsequently, the examination of the degradation products obtained at 480°C reveals a decrease in the quantity of all the species produced, particularly carbon monoxide and dioxide. However, with the subsequent increase of the temperature to 537°C, the amount of hydrocarbon volatiles detected becomes negligible, while the CO remains relatively constant, and a substantial increase is observed for the CO_2. This spectrum reflects the complete degradation of the polymer, involving the entire conversion to carbon monoxide and carbon dioxide, with a clear predominance of the latter.

Focusing on the nanocomposite, the remarkable effect of the nanoclay is clearly evident from the comparison with the thermogravimetric curves of the pristine EBA (Figure 3A). In fact, when the analysis is performed in an inert atmosphere, the T_{ONSET} of EBA/nanoclay is 379°C, quite similar to that of the matrix. On the other hand, three weight loss steps are distinguished, and T_{MAX} shifts at 473°C, involving an improvement of 22°C compared to pristine EBA. The noticed delay can be attributed to the presence of the nanoclays, that create a barrier to the volatile degradation products, acting at the same time as a thermal insulator [41, 42].

Looking at the behavior of the nanocomposite in oxidative atmosphere (Figure 3A), it can be noticed that the T_{ONSET} is to 327°C (i.e., 22°C higher than that of unfilled EBA tested in the same conditions). Besides, the temperature at which the degradation occurs with the maximum rate is 482°C, which is practically comparable to that of the nanocomposite analyzed in inert atmosphere. As a matter of fact, the obtained results highlighted that the introduction of the nanofillers is able to provide a complete protective action against the oxidative atmosphere, as the nanocomposite shows the same behavior as in inert environment. Consequently, it can be concluded that the incorporation of the nanoclays has effectively improved the thermal resistance in both inert and oxidative atmospheres when compared to unfilled EBA.

3.2 | Morphological Characterization of EBA/Nanoclay Films and Coated Samples

SEM analyses were performed to inspect the morphology of the produced samples and to evaluate the degree of dispersion and distribution of the nanoclay in the films obtained by the two different processing methods. In Figure 3A, the film formulated through compression molding shows well dispersed and evenly distributed nanoclay. The same result is observed for the cast-extruded sample (Figure 3B). However, in this case, a preferential orientation of the lamellae along the extrusion direction of the film can be undoubtedly recognized [43, 44].

Additionally, the section of the EBA/nanoclay_coating_CE specimen is presented in Figure 3C. The film applied to the surface of the blank EBA sample is easily distinguishable, and in particular, a very good adhesion between the coating and the underlying EBA substrate is clearly appreciable, with no voids or discontinuities at the interface.

3.3 | Combustion Behavior

The combustion behavior of all formulated EBA-based systems was evaluated through cone calorimeter tests with a heat flux of 35 kW/m^2. The curves of HRR and THR as a function of time of all investigated EBA-based systems are shown in Figure 4, while Table 3 lists the main evaluated parameters.

The EBA sample is characterized by a time to ignition of 53 ± 1 s, a flame out time of 267 ± 11 s and reaches a maximum value of HRR of 873 ± 59 kW/m2 after 189 ± 10 s. The bulk incorporation of 4 wt.% nanoclay results in the disappearance of the sharp HRR peak and consequently leads to a broader and flatter HRR curve. This is indicative of a slower, more controlled combustion and, therefore, enhanced flame-retardant properties. Specifically, the EBA/nanoclay_bulk sample exhibited a significant reduction of the peak heat release rate by approximately 50% (471 ± 27 kW/m^2), a modest increase of the time to ignition to 66 ± 7 s, and a substantial extension of the flame-out time to 472 ± 16 s. The flame retardant effect of the nanoclay is also evident in the THR graph (Figure 4B), where, due to the presence of the nanoclay, the slower growth of the total heat released can be appreciated from the lower slope of the curve. These results confirm what has already been widely reported in the literature regarding the mechanism and effectiveness of organoclays in improving the fire retardancy properties of polymers. In particular, as briefly anticipated in the introduction, it has been shown that the acidic sites present on the silicate layers (generated from the thermal degradation of the organo-modifiers) are able to catalyze the formation of a char-like layer on the material surface. This layer has a double effect. On one hand, it acts as a barrier to the mass transport of the volatile degradation products; besides, as a thermal shield, the char limits the further exposure of the polymer to heat and oxidative atmosphere. In addition, the acidic sites also catalyze dehydrogenation and crosslinking reactions of the polymer chains, thereby enhancing the material thermo-oxidative stability (as previously demonstrated by TGA analyses). Finally, a further contribution to flame retardancy arises from the physical barrier formed by the ablative reassembly of the silicate layers on the polymer surface [45–47].

For the EBA/nanoclay_bulk sample, because of pkHRR decrease, also FPI is lowered (Table 3), indicating an improvement in fire retardancy performance owing to the presence of the nanoclay. Regarding the FIGRA parameter, a slight increase of its value is actually observed in the presence of nanoclay, due to the earlier occurrence of the HRR peak.

The results obtained are similar to those reported in several studies on EVA [3, 48, 49]. For instance, Entezam et al. [17], upon adding 5 phr of nanoclay to an EVA matrix, observed a pkHRR reduction of about 50% and longer flame out time. Observing the values of total smoke release (Table 3), it can be seen that in the presence of nanoclay, this value is higher than the unfilled EBA. This can be correlated with the fact that nanoclay may disrupt the combustion process by forming a barrier to oxygen or slowing down the combustion rate, leading to incomplete combustion. As a consequence, soot and volatile organic compounds are produced, thus causing an increase of TSR. The larger smoke

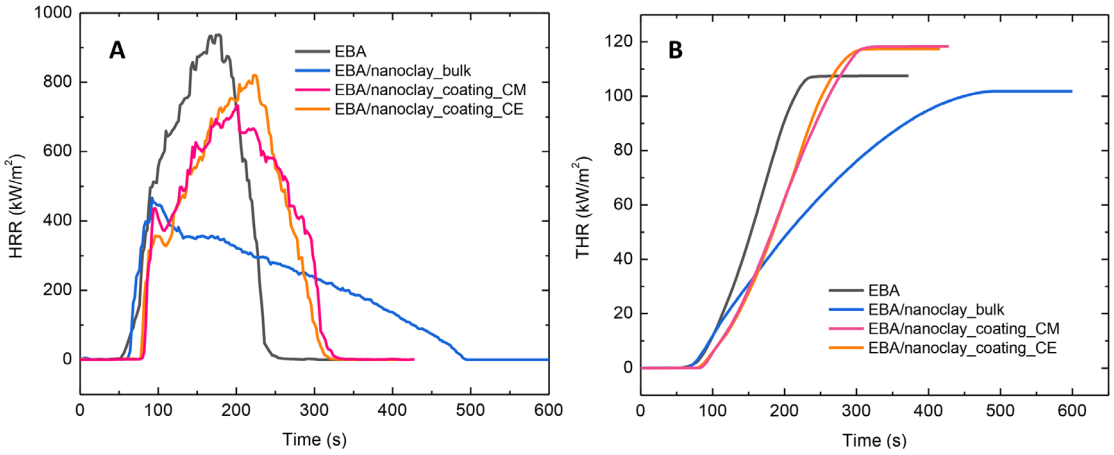

FIGURE 4 | (A) HRR and (B) THR as a function of time for EBA, EBA/nanoclay_bulk, EBA/nanoclay_coating_CM and EBA/nanoclay_coating_CE samples.

TABLE 3 | Cone calorimetry data and parameters of all investigated EBA-based systems.

Specimen	TTI (s)	Flameout Time (s)	pkHHR (kW/m²)	t peak (s)	THR (kW/m²)	TSR (m²/m²)	FPI (kW/m²s)	FIGRA (kW/m²s)
EBA	53 ± 1	267 ± 11	873 ± 59	189 ± 10	104 ± 6	1304 ± 76	16.4	4.6
EBA/nanoclay_bulk	66 ± 7	472 ± 16	471 ± 27	97 ± 4	101 ± 1	2084 ± 135	7.1	4.9
EBA/nanoclay_coating_CM	79 ± 2	320 ± 21	738 ± 62	205 ± 3	119 ± 1	1651 ± 38	9.3	3.6
EBA/nanoclay_coating_CE	79 ± 5	290 ± 16	880 ± 52	221 ± 12	118	1555 ± 54	11.2	4

production upon the introduction of nanoclay was also observed by Zhang et al. [50].

Having demonstrated the effectiveness of the bulk approach, the surface approach was then investigated using both the CM and CE films. It is important to note that the nanocomposite film applied as a surface layer was loaded with 4 wt.% nanoclay, but relative to the total weight of the sample, the actual nanofiller content was only 0.36 wt.%, approximately one-tenth of that used in the EBA/nanoclay_bulk samples. As shown in Figure 5A, compared to pristine EBA, the presence of the coatings results primarily in a 26 s delay of the TTI (50% increase), an extension of the flame-out time and a decrease of pkHRR of about 30%, along with a shift of the peak at higher times. These observations suggest that, despite the lower overall nanofiller content, localizing the nanoclay at the surface through the application of the film enables a more effective and rapid formation of the protective char layer, leading to a more pronounced TTI delay compared to the bulk approach and therefore to a slower propagation of the fire and improved fire safety. This assumption is further evidenced by the initial char formation times recorded for all the investigated samples prior to ignition. Specifically, while the unfilled EBA does not show char formation, in the case of the EBA/nanoclay_coating_CE sample, the time at which char formation starts (i.e., 35 s) is significantly lower than for the material obtained through bulk incorporation (i.e., 58 s), confirming the greater effectiveness of the coating strategy in promoting char formation.

The influence of the nanoclay arrangement and spatial distribution on the combustion behavior was also demonstrated by Colonna et al. [8]. In particular, it was shown that the annealing of an EVA/Cloisite20A nanocomposite at a temperature near its melting point led to lamellae exfoliation and promoted the early migration of clay toward the surface during combustion. This facilitated the formation of a thin lamellar film, which contributed to a delay of the ignition, resembling the effect observed in the coated samples object of this study. Specifically, in our case, combustion is effectively slowed until around 100 s and then, beyond this point, the HRR curve begins to resemble that of neat EBA, as the volatiles trapped inside reach a pressure high enough to rupture the thin surface char layer, thus ending the barrier effect and allowing the underlying polymer to continue burning. The delay in TTI achieved with the coatings confirms observations from a previous study [25], in which the use of an EVA-based coating containing 3 wt.% biochar led to a significant delay in ignition compared to the unfilled material, while the incorporation of 20 or 40 wt.% biochar even resulted in an advancement of ignition by 30 s. Furthermore, similarities can also be observed in terms of the reduction of pkHRR and the delay in time to peak upon the use of the coating.

The observed delay of TTI is an interesting result when considering the fact that many studies [51–54] show how the incorporation of nanoclay often leads to a reduction of the TTI and a more rapid increase of HRR due to accelerated decomposition of the polymer matrix promoted by the acidic sites on the layered silicates created by the decomposition of the organomodifier. As a result, the release of volatile combustibles occurs, advancing and initially accelerating the growth of HRR. However, by localizing the nanoclays at the sample surface, the effect of the organomodifiers is

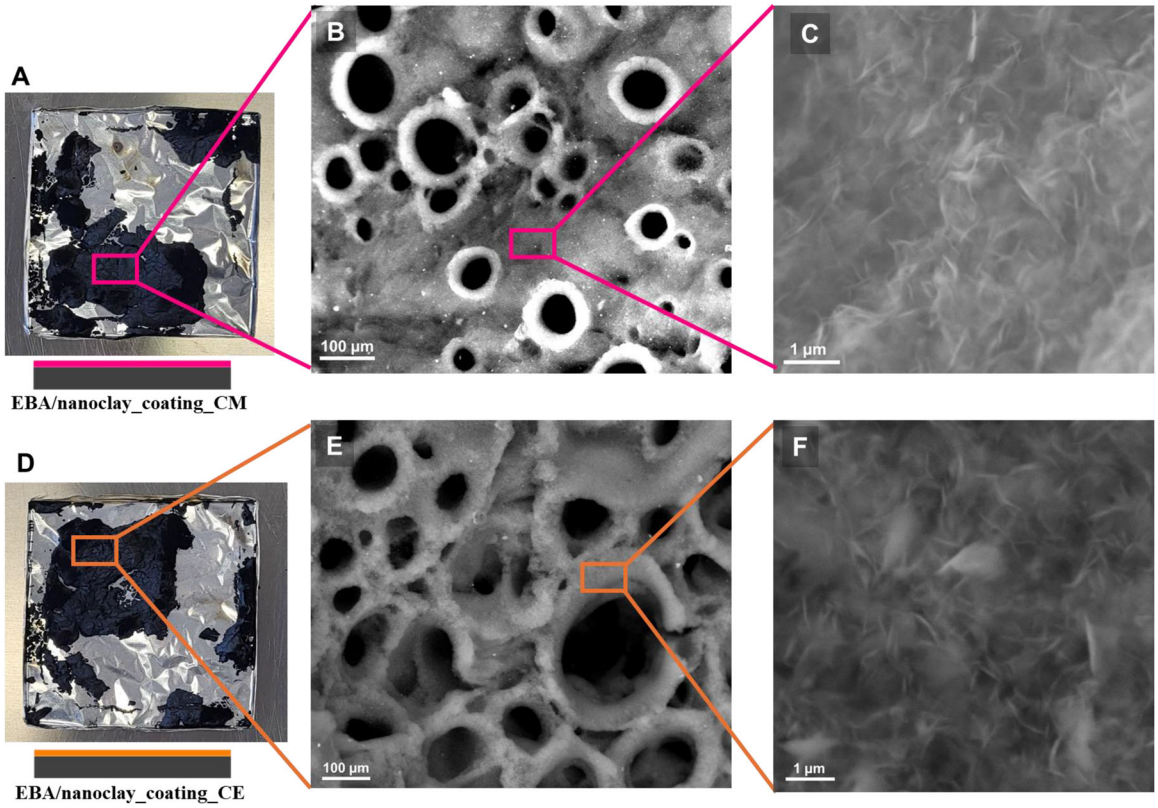

FIGURE 5 | Pictures and SEM micrograph of EBA/nanoclay_coating_CM (A,B,C) EBA/nanoclay_coating_CE (D,E,F) char residues after cone calorimeter test.

minimized owing to the faster and more efficient char formation, which mitigates the initial release of volatile compounds and provides a more controlled ignition process. The ability of the coating to delay the ignition is also evident in the THR curves (Figure 4B), where a shift to longer times can be observed. In this case, the final THR value is higher than that of pure EBA, as the presence of the coating results in a larger polymer content in the coated samples, specifically amounting to a 9.2% increase.

Besides, the surface approach results in the lowest FIGRA (Table 3), even when compared to the bulk nanocomposite, indicating a slower flame spread potential and improved fire safety [55]. Moreover, the lower FPI compared to unfilled EBA samples, provides further evidence of the effectiveness of the proposed approach. Regarding the values of total smoke release (Table 3), it can be observed that in the presence of the coating, these are intermediate between those of unfilled EBA and EBA/nanoclay_bulk. This is consistent, as the amount of nanoclay is lower than that present in the bulk samples, and the results confirm the fact that the higher the percentage of nanoclay in the sample, the higher the TSR and the lower the pkHRR values.

Finally, confirmation of the effective action of the nanoclay within the surface layer was also provided by the visual observation of the carbonaceous residues of the EBA/nanoclay samples obtained through the coating approach (Figure 5A,D). The SEM micrographs of the inner side of the char (Figure 5B,E) reveal from both residues a porous structure, which, as explained in the literature [56], originates from the rising bubbles of degradation products moving from the sample interior toward its surface through convective motion in the melt. As a result, the nanoclay lamellae migrate to the surface, where they act as a barrier. The occurrence of this phenomenon is demonstrated by the high magnification SEM micrographs depicted in Figure 5C,F, in which the presence of the nanoclay layers is clearly observable. In the case of the coating, this mechanism is facilitated by the localization of the nanoclay on the surface, allowing for a more rapid barrier effect and, consequently, a more effective delay in ignition time.

4 | Conclusion

This study has demonstrated the effectiveness of nanostructured films applied as surface layers in developing flame-retardant EBA-based systems. Initially, an EBA-based nanocomposite containing 4 wt.% nanoclay was produced through melt compounding, and the main thermal and rheological properties, as well as its morphology and thermal and thermo-oxidative behavior, were preliminarily assessed. Furthermore, through cone calorimetry tests, the effectiveness of the nanoclay in reducing the peak heat release rate and slowing polymer combustion was confirmed. Subsequently, a surface approach was investigated, and pre-prepared EBA + 4 wt.% nanoclay films (both compression molded and cast extruded) were hot-pressed onto the surface of unfilled EBA specimens, resulting in an overall nanofiller content of 0.36 wt.%. Cone calorimeter tests demonstrated that, regardless of the film-forming method, the surface confinement of the nanoclay, obtained through the coating approach, promoted a faster

and more efficient formation of a protective char layer, leading to an even greater delay in the time to ignition, compared to the bulk incorporation. Overall, the obtained results highlighted that the exploitation of a nanoclay-rich surface layer offers additional advantages: (i) the total amount of nanoclay in the specimen is only 0.36 wt.%, making it a highly efficient solution in terms of material usage; (ii) by localizing the nanoclay at the surface, the mechanical properties of the polymer matrix are expected to remain unaltered, preserving as an example its flexibility; (iii) due to the very low nanoclay content, the material recyclability is improved, as the coated material can be recycled in the same stream of the unfilled polymer, avoiding the concerns typically associated with high filler concentrations.

Acknowledgements

The authors thank Dr. Günter Beyer for fruitful discussion and Lucobit for supplying the materials.

Open access publishing facilitated by Politecnico di Torino, as part of the Wiley - CRUI-CARE agreement.

Conflicts of Interest

The authors declare no conflicts of interest.

Data Availability Statement

The data that support the findings of this study are available from the corresponding author upon reasonable request.

References

1. G. Camino and L. Costa, "Performance and Mechanisms of Fire Retardants in Polymers—A Review," *Polymer Degradation and Stability* 20 (1988): 271–294, https://doi.org/10.1016/0141-3910(88)90073-0.

2. F. Bellucci, G. Camino, A. Frache, and A. Sarra, "Catalytic Charring–Volatilization Competition in Organoclay Nanocomposites," *Polymer Degradation and Stability* 92 (2007): 425–436, https://doi.org/10.1016/j.polymdegradstab.2006.11.006.

3. M. Zanetti, T. Kashiwagi, L. Falqui, and G. Camino, "Cone Calorimeter Combustion and Gasification Studies of Polymer Layered Silicate Nanocomposites," *Chemistry of Materials* 14 (2002): 881–887, https://doi.org/10.1021/cm011236k.

4. H. O. Pastore, A. Frache, E. Boccaleri, L. Marchese, and G. Camino, "Heat Induced Structure Modifications in Polymer-Layered Silicate Nanocomposites," *Macromolecular Materials and Engineering* 289 (2004): 783–786, https://doi.org/10.1002/mame.200400109.

5. G. Malucelli, F. Carosio, J. Alongi, A. Fina, A. Frache, and G. Camino, "Materials Engineering for Surface-Confined Flame Retardancy," *Materials Science and Engineering: R: Reports* 84 (2014): 1–20, https://doi.org/10.1016/j.mser.2014.08.001.

6. S. Liang, N. M. Neisius, and S. Gaan, "Recent Developments in Flame Retardant Polymeric Coatings," *Progress in Organic Coatings* 76 (2013): 1642–1665, https://doi.org/10.1016/j.porgcoat.2013.07.014.

7. W. Wang, Y. Liu, Z. Han, and Q. Wang, "A Coating Method Combined With Bulk Addition for Efficient Flame Retardant Thermoplastic Polyolefin Sheet Material," *Polymer Degradation and Stability* 174 (2020): 109093, https://doi.org/10.1016/j.polymdegradstab.2020.109093.

8. S. Colonna, F. Cuttica, and A. Frache, "Aging of EVA/Organically Modified Clay: Effect on Dispersion, Distribution and Combustion Behavior," *Polymer Degradation and Stability* 107 (2014): 184–187, https://doi.org/10.1016/j.polymdegradstab.2014.05.019.

9. S. Matta, M. Bartoli, A. Frache, and G. Malucelli, "Investigation of Different Types of Biochar on the Thermal Stability and Fire Retardance of Ethylene-Vinyl Acetate Copolymers," *Polymers* 13 (2021): 1256, https://doi.org/10.3390/polym13081256.

10. E. Gallo, B. Schartel, D. Acierno, F. Cimino, and P. Russo, "Tailoring the Flame Retardant and Mechanical Performances of Natural Fiber-Reinforced Biopolymer by Multi-Component Laminate," *Composites Part B: Engineering* 44 (2013): 112–119, https://doi.org/10.1016/j.compositesb.2012.07.005.

11. W. Tabaka and B. Schartel, "Less is More: Optimised Fire Performance in Glass Fibre-Reinforced Polybutylene Terephthalate Laminates With Concentrated Flame Retardant Top layer," *Composites Part C: Open Access* 16 (2025): 100577, https://doi.org/10.1016/j.jcomc.2025.100577.

12. Carosio, G. Laufer, J. Alongi, G. Camino, and J. C. Grunlan, "Layer-By-Layer Assembly of Silica-Based Flame Retardant Thin Film on PET Fabric," *Polymer Degradation and Stability* 96 (2011): 745–750, https://doi.org/10.1016/j.polymdegradstab.2011.02.019.

13. G. Camino, L. Costa, and G. Martinasso, "Intumescent Fire-Retardant Systems," *Polymer Degradation and Stability* 23 (1989): 359–376, https://doi.org/10.1016/0141-3910(89)90058-X.

14. G. Camino, R. Sgobbi, A. Zaopo, S. Colombier, and C. Scelza, "Investigation of Flame Retardancy in EVA," *Fire and Materials* 24 (2000): 85–90, https://doi.org/10.1002/1099-1018(200003/04)24:2⟨85.

15. A. Durin-France, L. Ferry, J. M. Lopez Cuesta, and A. Crespy, "Magnesium Hydroxide/Zinc Borate/Talc Compositions as Flame-Retardants in EVA Copolymer," *Polymer International* 49 (2000): 1101–1105, https://doi.org/10.1002/1097-0126(200010)49.

16. Y. Y. Yen, H. T. Wang, and W. J. Guo, "Synergistic Flame Retardant Effect of Metal Hydroxide and Nanoclay in EVA Composites," *Polymer Degradation and Stability* 97 (2012): 863–869, https://doi.org/10.1016/j.polymdegradstab.2012.03.043.

17. M. Entezam, H. A. Khonakdar, S. M. A. Jafari, and M. Otadi, "Thermal Stability And Flammability of Ethylene Vinyl Acetate Copolymers in Presence of Nanoclay and A Halogen-Free Flame Retardant," *Journal of Vinyl and Additive Technology* 23 (2017): E92–E98, https://doi.org/10.1002/vnl.21566.

18. Y. Feng, H. Wang, B. Zhang, et al., "Effect of Different Surface Modifiers on The Flame Retardancy of Ethylene-Vinyl Acetate Copolymer/Polyethylene/Magnesium Hydroxide Composite Systems," *Journal of Applied Polymer Science* 141 (2024): 56061, https://doi.org/10.1002/app.56061.

19. X. Yang, X. Dong, M. Liu, et al., "Efficient Flame-Retarded Ethylene Vinyl Acetate Composite Containing Microencapsulated Expandable Graphite And Polyphosphoric Acid," *Polymer Degradation and Stability* 227 (2024): 110904, https://doi.org/10.1016/j.polymdegradstab.2024.110904.

20. B. Sultan and E. Sörvik, "Thermal Degradation of EVA and EBA—A Comparison. I. Volatile Decomposition Products," *Journal of Applied Polymer Science* 43 (1991): 1737–1745, https://doi.org/10.1002/app.1991.070430917.

21. N. Huang and J. Wang, "A TGA-FTIR Study on the Effect of $CaCO_3$ on the Thermal Degradation of EBA Copolymer," *Journal of Analytical and Applied Pyrolysis* 84 (2009): 124–130, https://doi.org/10.1016/j.jaap.2009.01.001.

22. L. Karlsson, A. Lundgren, J. Jungqvist, and T. Hjertberg, "Influence of Melt Behaviour on The Flame Retardant Properties of Ethylene Copolymers Modified With Calcium Carbonate and Silicone Elastomer," *Polymer Degradation and Stability* 94 (2009): 527–532, https://doi.org/10.1016/j.polymdegradstab.2009.01.025.

23. S. P. S. Ribeiro, L. R. M. Estevão, and R. S. V. Nascimento, "Effect of Clays on the Fire-Retardant Properties of a Polyethylenic Copolymer Containing Intumescent Formulation," *Science and Technology of Advanced Materials* 9 (2008): 024408, https://doi.org/10.1088/1468-6996/9/2/024408.

24. X. Huo, B. Wu, Y. Lou, et al., "Synergistic Effect of Ammonium Polyphosphate and Silicone Macromolecular Charring Agent on Improving Flame Retardancy and Mechanical Properties of Ethylene-Butyl

Acrylate Copolymer Composites," *Journal of Polymer Materials* 42 (2025): 517–530, https://doi.org/10.32604/jpm.2025.065320.

25. S. Matta, M. Bartoli, R. Arrigo, A. Frache, and G. Malucelli, "Flame Retardant Potential of Tetra Pak®-Derived Biochar for Ethylene-Vinyl-Acetate Copolymers," *Composites Part C: Open Access* 8 (2022): 100252, https://doi.org/10.1016/j.jcomc.2022.100252.

26. S. Sancho-Querol, A. J. Yáñez-Pacios, and J. M. Martín-Martínez, "New Binary Blends of Ethylene-Co-N-Butyl Acrylate (Eba) Copolymer And Low Molecular Weight Rosin Ester Resin With Potential as Pressure Sensitive Adhesives," *Materials* 11 (2018): 2037, https://doi.org/10.3390/ma11102037.

27. B. Schartel and T. R. Hull, "Development of Fire-Retarded Materials—Interpretation of Cone Calorimeter Data," *Fire and Materials* 31 (2007): 327–354, https://doi.org/10.1002/fam.949.

28. A. Morro, F. Catalina, T. Corrales, J. L. Pablos, I. Marin, and C. Abrusci, "New Blends of Ethylene-Butyl Acrylate Copolymers With Thermoplastic Starch. Characterization and Bacterial Biodegradation," *Carbohydrate Polymers* 149 (2016): 68–76, https://doi.org/10.1016/j.carbpol.2016.04.075.

29. D. S. Chaudhary, R. Prasad, R. K. Gupta, and S. N. Bhattacharya, "Clay Intercalation and Influence on Crystallinity of EVA-Based Clay Nanocomposites," *Thermochimica Acta* 433 (2005): 187–195, https://doi.org/10.1016/j.tca.2005.02.031.

30. M. T. Albdiry, B. F. Yousif, H. Ku, and K. T. Lau, "A Critical Review on the Manufacturing Processes in Relation to the Properties of Nanoclay/Polymer Composites," *Journal of Composite Materials* 47 (2013): 1093–1115, https://doi.org/10.1177/0021998312445592.

31. A. Rajan, P. Upadhyaya, N. Chand, and V. Kumar, "Effect of Nanoclay on the Thermal Properties of Compatibilized Ethylene Vinyl Acetate Copolymer/High-Density Polyethylene Blends," *Journal of Thermoplastic Composite Materials* 27 (2014): 650–662, https://doi.org/10.1177/0892705712453157.

32. M. C. Mistretta, L. Botta, R. Arrigo, F. Leto, G. Malucelli, and F. P. La Mantia, "Bionanocomposite Blown Films: Insights on the Rheological and Mechanical Behavior," *Polymers* 13 (2021): 1167, https://doi.org/10.3390/polym13071167.

33. B. Vergnes, "The Use of Apparent Yield Stress to Characterize Exfoliation in Polymer Nanocomposites," *International Polymer Processing* 26 (2011): 229–232, https://doi.org/10.3139/217.2462.

34. B. Sultan and E. Sörvik, "Thermal Degradation of EVA and EBA—A comparison. II. Changes in Unsaturation and Side Group Structure," *Journal of Applied Polymer Science* 43 (1991): 1747–1759, https://doi.org/10.1002/app.1991.070430918.

35. B. Sultan and E. Sörvik, "Thermal Degradation of EVA and EBA—A Comparison. III. Molecular Weight Changes," *Journal of Applied Polymer Science* 43 (1991): 1761–1771, https://doi.org/10.1002/app.1991.070430919.

36. M. Gardette, A. Perthue, J. L. Gardette, et al., "Photo- And Thermal-Oxidation of Polyethylene: Comparison of Mechanisms and Influence of Unsaturation Content," *Polymer Degradation and Stability* 98 (2013): 2383–2390, https://doi.org/10.1016/j.polymdegradstab.2013.07.017.

37. J. Almond, P. Sugumaar, M. N. Wenzel, G. Hill, and C. Wallis, "Determination of the Carbonyl Index of Polyethylene and Polypropylene Using Specified Area Under Band Methodology With ATR-FTIR Spectroscopy," *e-Polymers* 20 (2020): 369–381, https://doi.org/10.1515/epoly-2020-0041.

38. J. London, "Infrared Spectra of Carbon Monoxide, Carbon Dioxide, Nitric Oxide, Nitrogen Dioxide, Nitrous Oxide, and Nitrogen Adsorbed on Copper Oxide," *Journal of Catalysis* 31 (1973): 32–40, https://doi.org/10.1016/0021-9517(73)90267-4.

39. P. Wakwella, A. R. W. McKellar, and N. Moazzen-Ahmadi, "Infrared Spectra of Both Isomers of CO_2 -CO in the CO_2v_3 Region," *Molecular Physics* 119 (2021): 1936251, https://doi.org/10.1080/00268976.2021.1936251.

40. E. M. Köck, M. Kogler, T. Bielz, B. Klötzer, and S. Penner, "In Situ FT-IR Spectroscopic Study of CO_2 and CO Adsorption on Y_2O_3 , ZrO_2 , and Yttria-Stabilized ZrO_2," *The Journal of Physical Chemistry C* 117 (2013): 17666–17673, https://doi.org/10.1021/jp405625x.

41. N. Karimpour-Motlagh, H. A. Khonakdar, S. M. A. Jafari, et al., "Influence of Polypropylene and Nanoclay on Thermal and Thermo-Oxidative Degradation of Poly(Lactide Acid): TG-FTIR, TG-DSC Studies and Kinetic Analysis," *Thermochimica Acta* 691 (2020): 178709, https://doi.org/10.1016/j.tca.2020.178709.

42. J. Golebiewski and A. Galeski, "Thermal Stability of Nanoclay Polypropylene Composites by Simultaneous DSC and TGA," *Composites Science and Technology* 67 (2007): 3442–3447, https://doi.org/10.1016/j.compscitech.2007.03.007.

43. R. Arrigo, G. Malucelli, and F. P. La Mantia, "Effect of the Elongational Flow on the Morphology and Properties of Polymer Systems: A Brief Review," *Polymers* 13 (2021): 3529, https://doi.org/10.3390/polym13203529.

44. S. Morimune-Moriya, M. Kotera, and T. Nishino, "Alignment Control of Clay and its Effect on Properties of Polymer Nanocomposites," *Polymer* 256 (2022): 125202, https://doi.org/10.1016/j.polymer.2022.125202.

45. M. Zanetti, T. Kashiwagi, L. Falqui, and G. Camino, "Cone Calorimeter Combustion and Gasification Studies of Polymer Layered Silicate Nanocomposites," *Chemistry of Materials* 14 (2002): 881–887, https://doi.org/10.1021/cm011236k.

46. S. Bocchini and G. Camino, "Flammability and Thermal Stability in Clay/Polyester Nano-Biocomposites," *Green Energy Technology* 50 (2012): 265–285, https://doi.org/10.1007/978-1-4471-4108-2_10.

47. M. Zanetti, G. Camino, and R. Mülhaupt, "Combustion Behaviour of EVA/Fluorohectorite Nanocomposites," *Polymer Degradation and Stability* 74 (2001): 413–417, https://doi.org/10.1016/S0141-3910(01)00178-1.

48. S. Duquesne, C. Jama, M. L. Bras, R. Delobel, P. Recourt, and J. M. Gloaguen, "Elaboration of EVA–Nanoclay Systems—Characterization, Thermal Behaviour and Fire Performance," *Composites Science and Technology* 63 (2003): 1141–1148, https://doi.org/10.1016/S0266-3538(03)00035-6.

49. G. Beyer, "Flame Retardancy of Nanocomposites—From Research to Technical Products," *Journal of Fire Sciences* 23 (2005): 75–87, https://doi.org/10.1177/0734904105048591.

50. J. Zhang, J. Hereid, and M. Hagen, et al., "Effects of Nanoclay and Fire Retardants on Fire Retardancy of a Polymer Blend of EVA and LDPE," *Fire Safety Journal* 44 (2009): 504–513, https://doi.org/10.1016/j.firesaf.2008.10.005.

51. M. Zanetti, G. Camino, D. Canavese, A. B. Morgan, F. J. Lamelas, and C. A. Wilkie, "Fire Retardant Halogen–Antimony–Clay Synergism in Polypropylene Layered Silicate Nanocomposites," *Chemistry of Materials* 14 (2002): 189–193, https://doi.org/10.1021/cm011124t.

52. H. J. Ryu, J. H. Lee, J. Y. Choi, G. Choi, N. S. Rejinold, and J. H. Choy, "Composite Nanoarchitectonics With Ionic Clay Nanofillers-Embedded Polypropylene for Efficient Flame Retardance," *Applied Clay Science* 246 (2023): 107181, https://doi.org/10.1016/j.clay.2023.107181.

53. A. Fina and G. Camino, "Ignition Mechanisms in Polymers and Polymer Nanocomposites," *Polymers for Advanced Technologies* 22 (2011): 1147–1155, https://doi.org/10.1002/pat.1971.

54. J. Gilman, "Flammability and Thermal Stability Studies of Polymer Layered-Silicate (clay) Nanocomposites," *Applied Clay Science* 15 (1999): 31–49, https://doi.org/10.1016/S0169-1317(99)00019-8.

55. C. Nyambo, E. Kandare, and C. A. Wilkie, "Thermal Stability and Flammability Characteristics of Ethylene Vinyl Acetate (EVA) Composites Blended With a Phenyl Phosphonate-Intercalated Layered Double Hydroxide (LDH), Melamine Polyphosphate and/or Boric Acid," *Polymer Degradation and Stability* 94 (2009): 513–520, https://doi.org/10.1016/j.polymdegradstab.2009.01.028.

56. T. Kashiwagi, R. H. Harris, X. Zhang, et al., "Flame Retardant Mechanism of Polyamide 6–Clay Nanocomposites," *Polymer* 45 (2004): 881–891, https://doi.org/10.1016/j.polymer.2003.11.036.